*Int. J. Heat Mass Transfer.* Vol. 32, No. 12, pp. 2421–2434, 1989
Printed in Great Britain

0017–9310/89 $3.00 + 0.00


# A multi-dimensional model of momentum and mass transfer in the liver

CHARLES Y. C. LEE and BORIS RUBINSKY†
Department of Mechanical Engineering, University of California at Berkeley, Berkeley, CA 94720, U.S.A.

(*Received* 8 *September* 1988 *and in final form* 31 *March* 1989)

**Abstract**—A new concept in modeling multi-dimensional fluid flow and mass transfer in the liver utilizing principles from porous media theory is introduced. From this model, a distribution of the pressure and velocity values is obtained for fluid in the microvasculature. The velocities for the fluid are then incorporated into a multi-dimensional conservation of chemical species equation. A distribution of the chemical species concentration in the fluid and the tissue is then determined using an equation which describes the mass transfer process across the cell membrane. Several parametric studies which included the effects of the vascular architecture on pressure and flow distribution, and the response to a step change in the inlet chemical species concentration are conducted to determine the sensitivity of the model.

## INTRODUCTION

MAJOR functions of the liver include effective uptake of chemical substances, their subsequent storage, metabolism, biotransformation, and distribution to the blood and bile [1]. The rate at which the liver performs these functions is of importance in various disciplines. In liver physiology, these rates are important in characterizing various chemical species and in predicting hepatic response to various external stimuli. In pharmacology, the quantitative uptake of drugs is important in determining dosage requirements for drug delivery. In treating liver diseases such as hepatitis, cancer, and cirrhosis, determining the drug distribution within the liver becomes important because treatment is effective only if affected areas receive adequate dosage. For example, treatment of Hepatitis B Virus (HBV) with antiviral agents has been effective in suppressing virus replication. However, in most cases this effect has been transient and active virus replication resumed after withdrawal of the drug [2]. An inadequate dosage of drug to the affected area could be one possible factor among a number of others which may allow viral replication to resume.

Mass transfer of chemical species into and out of the hepatocytes (liver cells) occurs at the level of the hepatic acinus, a repetitive microvascular unit of hepatic parenchyma [3]. The acinus in Fig. 1(a) is a complex multi-dimensional array of hepatocytes, sinusoids (capillary network), portal triads (terminal portal venule, terminal hepatic arteriole, and bile duct), and hepatic venules [4]. Mass transfer at the microcirculatory level between fluid and cells has been shown to be complex and nonuniform [5]. Concentration gradients of chemical species vary nonuniformly both in the fluid and tissue between the portal triads and the terminal hepatic venule [4, 5]. Fluid flow through the hepatic acinus is also complex. From a global view, flow appears to be unidirectional occurring from the terminal portal vein and hepatic artery through the sinusoids to the peripheral hepatic vein. However, at the microcirculatory level, this is not the case. Numerous branches and interconnections [6] between sinusoids coupled with the irregular geometry of the acinus increases the complexity of fluid flow.

At present, there are no models which attempt to simulate mass transfer of chemical species between fluid in the sinusoids and the hepatocytes at the microcirculatory level. Most mass transfer models of the liver do not study the details of the microvasculature. Currently, there are four models widely used to simulate uptake of chemical species in the liver: (a) the well-stirred or venous equilibrium model [7], (b) the parallel tube or sinusoidal perfusion model [8], (c) the distributed model [9, 10], and (d) the dispersion model [11]. In general, these models attempt to understand input/output relationships of chemical species utilizing indicator-dilution curves obtained from data of venous outflow following the simultaneous injection of tracers into the arterial or portal inflow. The well-stirred model [7] assumes all cells in the liver see the same concentration simultaneously. This model is effective for analyzing responses to a step change in chemical species at the inlet flow. However, it is not consistent with the observed behavior of outputs following an impulse input of chemical species [11]. The parallel tube model [8] assumes that the liver can be represented as a single cylindrical tube of constant radius. Under this assumption, the response to an impulse input of a non-permeating chemical species is an impulse at the output, as opposed to Gaussian-like curves obtained from experimental results [9, 10]. The

† Author to whom correspondence should be addressed.

## NOMENCLATURE

| | |
|---|---|
| $C$ | concentration of chemical species |
| $d_s$ | average diameter of sinusoids |
| $D$ | diffusion coefficient of chemical species |
| $h$ | time step size |
| $k$ | hydraulic permeability of the porous media |
| $L_s$ | characteristic length of a sinusoid |
| $M$ | $n \times n$ stiffness matrix |
| $M_0$ | specified mass flux |
| $n$ | normal direction |
| $P$ | local fluid pressure |
| $P_s$ | cell membrane permeability |
| $Pe_m$ | mass transfer Peclet number |
| $Q$ | $n \times n$ matrix |
| $Re_{d_s}$ | Reynolds number in the sinusoids |
| $S$ | $n \times n$ matrix |
| $S_a$ | surface area of hepatocytes |
| $t$ | time |
| $u, v, w$ | fluid velocity in the $x$-, $y$-, and $z$-directions |
| $V$ | volume of sinusoids and tissue |
| $x, y, z$ | Cartesian coordinates. |

Greek symbols

| | |
|---|---|
| $\Gamma$ | boundary of the domain |
| $\theta$ | porosity of the porous media |
| $\phi$ | interpolation function |
| $\Omega$ | domain of the acinus. |

Subscripts

| | |
|---|---|
| 0 | initial or reference values |
| f | fluid properties |
| $i$ | summation, time index |
| $n$ | dimension of the system |
| s | properties in the sinusoids |
| t | properties in the tissue |
| $x, y, z$ | properties in the $x$-, $y$-, and $z$-directions under vector parameter. |

Superscripts

| | |
|---|---|
| $i$ | index |
| * | dimensionless variable. |

distributed model [9, 10] attempts to simulate the morphological arrangement of capillaries in the liver by utilizing a mathematical distribution of the parallel model whereby the capillaries have variable length. Distributed models exhibit some limitations since they do not permit lateral exchange of solute between regions having different velocities or direction of flow. The dispersion model [11] attempts to simulate the whole liver as a packed bed. Thus, it includes an axial dispersion term to represent the non-ideal flow in the

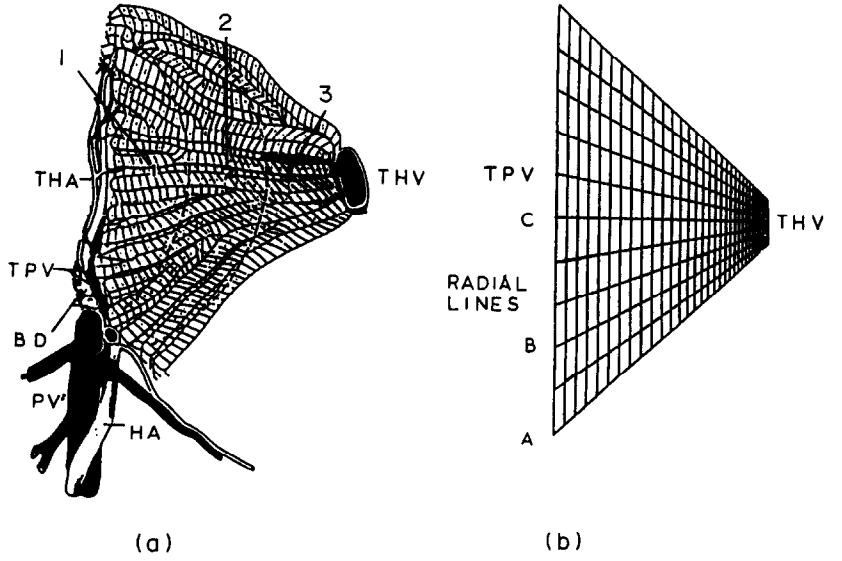


FIG. 1. (a) Hepatic acinus: PV, portal vein; HA, hepatic artery; portal triad (BD, bile duct; TPV, terminal portal venule; THA, terminal hepatic arteriole); S, sinusoids; H, hepatocytes; THV, terminal hepatic venule: 1, 2, and 3 designate the different zones in the acinus. (Published with permission from J. J. Gumucio, Functional and anatomic heterogeneity in the liver acinus: impact on transport, *Am. J. Physiol.* **244** (Gastrointest. Liver Physiol., 7), G578–G582 (1983).) (b) Finite element grid simulating hepatic acinus. Longer base represents a terminal portal venule (TPV), and shorter base represent a terminal hepatic venule (THV). A, B, and C indicate the radial lines along which pressure, velocity, and concentration are plotted.

conservation of mass equation. Fluid in the dispersion model and in the other models is characterized as a constant bulk velocity through the liver. Given branching and interconnections among sinusoids, a constant velocity may not describe the flow patterns accurately. In general, these models give useful information from output data about hepatic clearance; however, they cannot predict the concentration distribution of chemical species relative to position in the hepatic acinus following their uptake.

The limitations of current models and the need for a more accurate understanding of the concentration distribution in the liver have led us to the development of a new concept in the modeling of fluid flow and mass transfer in the liver acinus. Well-established studies show that within the acinus approximately 80% of the volume is composed of hepatocytes and the rest by extracellular fluid [1]. Morphological studies and analysis with silicon rubber casts also show that the sinusoids from richly anastomotic channels [6], indicating that fluid flow through the acinus traverses a tortuous path. From these observations, the liver acinus can be characterized as a porous bed of hepatocytes. Our new model applies fluid flow and mass transfer principles from porous media theory to the hepatic acinus. This method can be used to determine local velocities and pressure. The velocities can then be incorporated into the general conservation of chemical species equation for chemical species in the fluid. Then coupled with an equation governing mass transfer across the cell membrane for a given chemical species, a concentration distribution for the species can be determined for the fluid and the tissue.

The advantage of using porous media theory is that the complexity of the acinus can be modeled relatively easily. This is done by introducing certain average physiological parameters (i.e. 'hydraulic permeability', porosity) which describe the local physical properties within the acinus. In addition to presenting the new model, the finite element method is used to simulate fluid flow and mass transfer in a realistic geometric representation of the liver acinus. To illustrate this model utilizing the finite element method, we apply the analysis to a simplified two-dimensional representation of the hepatic acinus.

## ANALYSIS

The derivation of the fundamental equations for the analysis of momentum (fluid flow) and mass transfer in the liver acinus modeled as a porous media will be presented. Based on scanning electron micrographs of the structure [12], the hepatic acinus can be characterized as a bed of porous material. A porous medium is defined as any material that contains pores and/or interconnected channels [6]. Fluid flow in this medium is characterized by the 'hydraulic permeability' of the vasculature and the pressure drop across it. The 'hydraulic permeability' of the vasculature to a specific fluid is a measure of resistance to flow, and is a function of the porosity (ratio of flow area/total area), the tortosity (ratio of path length/direction length), and the viscosity of the fluid.

*Momentum transfer (fluid flow) analysis*

The condition for utilizing the porous media theory for the momentum transfer (fluid flow) analysis is that the typical Reynolds number, $Re_{d_s}$, $(u_0 d_s/v)$ for flow in the porous media must be less than one [13]. When the value of the Reynolds number is less than one, viscous forces dominate and thus the fluid can be assumed to flow parallel to the walls of the channel. In addition, as fluid passes through the tortuous channels no eddies develop as a result of sharp curves or corners. Velocity profiles within the sinusoids are assumed to be flat and nonvarying in the radial direction. The equations governing flow in a three-dimensional porous material can then be obtained from Darcy's law [13]

$$u(x,y,z) = k_x(x,y,z)\frac{\partial P}{\partial x} \tag{1a}$$

$$v(x,y,z) = k_y(x,y,z)\frac{\partial P}{\partial y} \tag{1b}$$

$$w(x,y,z) = k_z(x,y,z)\frac{\partial P}{\partial z}. \tag{1c}$$

The velocities $u$, $v$, and $w$, are local velocities defined in terms of the derivatives of the local pressure $P$ in different Cartesian coordinates, $x$, $y$, and $z$. The hydraulic permeabilities $k_x$, $k_y$, and $k_z$ are only a function of position within the domain. Therefore, a local change in architecture of sinusoids can be incorporated into the model.

Since the fluid is incompressible, the porous medium does not deform for small pressure changes, and the flow is steady the continuity equations for fluid flow reduce to [14]

$$\frac{\partial u}{\partial x} + \frac{\partial v}{\partial y} + \frac{\partial w}{\partial z} = 0. \tag{2}$$

Substituting the expressions for the velocities, equation (1), into the continuity equation (2), the equation for the pressure distribution in the liver acinus becomes

$$\frac{\partial}{\partial x}\left(k_x\frac{\partial P}{\partial x}\right) + \frac{\partial}{\partial y}\left(k_y\frac{\partial P}{\partial y}\right) + \frac{\partial}{\partial z}\left(k_z\frac{\partial P}{\partial z}\right) = 0 \tag{3}$$

in $\Omega(x,y,z)$ where $\Omega$ is the domain. Typical boundary conditions consist of

$$P(\Gamma_0) = P_0 \text{ specified pressure on } \Gamma_0$$

and

$$\frac{\partial P(\Gamma_1)}{\partial n} = V_0 \text{ specified fluid flow velocity on } \Gamma_1$$

where $\Gamma_0 \cup \Gamma_1$ specifies the boundary. With knowledge of the hydraulic permeabilities, these equations

can be solved to determine local values of pressure for any three-dimensional geometry of the liver acinus. Then, the local fluid velocities can be determined from Darcy's law, equation (1).

*Transport mass transfer analysis*

The transient mass transfer analysis will atempt to determine the distribution of chemical species both in the fluid and in the tissue. This will involve the coupling of the general transient conservation of chemical species equation in the fluid with an equation governing mass transfer of the species across the cell membrane. The diffusion–convection equation for conservation of chemical species, $c_f$, in the fluid can be established from a macroscopic mass balance in a control volume that contains blood vessels and surrounding tissue

$$\frac{\partial}{\partial x}\left(D_x\frac{\partial C_f}{\partial x}\right)+\frac{\partial}{\partial y}\left(D_y\frac{\partial C_f}{\partial y}\right)+\frac{\partial}{\partial z}\left(D_z\frac{\partial C_f}{\partial z}\right)+u\frac{\partial C_f}{\partial x}+v\frac{\partial C_f}{\partial y}+w\frac{\partial C_f}{\partial z}=\frac{\partial}{\partial t}\left(C_f\frac{V_t}{V_f}C_t\right)\text{ in }\Omega \quad (4)$$

with the initial and typical boundary conditions of

$$C_f(\Omega,0)=C_0(\Omega)\text{ specified initial concentration}$$

$$C_f(\Gamma_0,t)=C_f(t)\text{ specified concentration on }\Gamma_0$$

$$\frac{\partial C_f(\Gamma_1,t)}{\partial n}=M_0(t)\text{ specified mass flux on }\Gamma_1$$

where $\Omega$ is the domain and $\Gamma_0\cup\Gamma_1$ specifies the boundary. This equation includes the diffusivities of the chemical species, $D_x$, $D_y$, and $D_z$, and the velocities $u$, $v$, and $w$ obtained from the fluid flow analysis. The term

$$\frac{\partial}{\partial t}\left(\frac{V_t}{V_f}C_t\right)$$

is the net change in the fluid chemical species concentration exchanging with the tissue.

The mass transfer Peclet number, $Pe_m$, $(u_0L_s/D_s)$ is defined as a ratio between two modes of species transport: convection and diffusion [15]. When the Peclet number is greater than one, convection dominates the conservation of chemical species equation (4) and the equation reduces to

$$u\frac{\partial C_f}{\partial x}+v\frac{\partial C_f}{\partial y}+w\frac{\partial C_f}{\partial z}=\frac{\partial}{\partial t}\left(C_f+\frac{V_t}{V_f}C_t\right). \quad (5)$$

This reduction requires a change in the order of the boundary conditions to be consistent with the physics of the problem. The condition becomes

$$C_f(\Gamma_0,t)=C_{f0}(t).$$

The second transient term in equations (4) and (5) is associated with the net loss or gain in chemical species in the perfusing fluid per unit volume to the surrounding tissue. The net change in chemical species can be associated with a number of mechanisms such as: (1) simple diffusion across the cell membrane, (2) metabolism of the chemical substrate, or (3) osmotic transients caused by high species concentration. The simple diffusion of nonmetabolites into cells is governed by Fick's law and can be implemented fairly easily [16]. The Michaelis–Menten law governs the rate of biochemical metabolism for various species [17, 18]. These relative rates can affect the steady-state concentration of the chemical species in the tissue significantly. For species movement due to osmotic transients, principles derived from irreversible thermodynamics can be applied [19].

In order to illustrate the method of analysis, we will analyze simple diffusion of nonmetabolites as the mode for mass transfer across the cell membrane from the fluid. This process is then governed by Fick's law

$$\frac{\partial C_t(x,y,z,t)}{\partial t}=\frac{P_sS_A}{V_t}(C_f(x,y,z,t)-C_t(x,y,z,t)) \quad (6)$$

where $C_t$ and $C_f$ are the concentration of the species in the tissue and the fluid, respectively, $P_s$ the species permeability across the cell membrane, $S_A$ the surface area of the tissue, and $V_t$ the volume of the tissue. Based on these sets of equations (1)–(6), momentum and mass transport of chemical species through the acinus can be calculated and local values of pressure, velocity, and concentrations provided.

## NUMERICAL ANALYSIS

The equations which couple momentum and mass transfer through the hepatic acinus with mass transport across the cell membrane form a set of boundary value problems. These problems can be solved numerically using the finite element method (FEM) [20]. The advantage for using such a method over others is its adaptability to real geometries. A standard procedure for implementing the finite element method is presented.

*Finite element method for momentum transfer*

The Galerkin formulation of the momentum transfer problem will be briefly presented. The formulation is well known and the details on the derivation can be found in numerous texts (see ref. [20]). We let

$$P(x,y,z)\approx P_n(x,y,z)=\sum_{i=1}^{n}P_i\phi_i(x,y,z)=\boldsymbol{\phi}^{\mathrm{T}}\mathbf{P}_n \quad (7)$$

and the test function

$$\delta P_n=\sum_{i=1}^{n}\delta P_i\phi_i(x,y,z)=\boldsymbol{\phi}^{\mathrm{T}}\delta\mathbf{P}_n$$

where $\phi_i(x,y,z)$ is the interpolation function and $\boldsymbol{\phi}$, $\mathbf{P}_n$, and $\delta\mathbf{P}_n$ are $n\times 1$ vectors. Upon integration of

equation (3) over the domain $\Omega$, we obtain the matrix equation

$$\delta\mathbf{P}^{\mathrm{T}}\left[\int_{\Omega}(k_x\boldsymbol{\phi}_x\boldsymbol{\phi}_x^{\mathrm{T}}+k_y\boldsymbol{\phi}_y\boldsymbol{\phi}_y^{\mathrm{T}}+k_z\boldsymbol{\phi}_z\boldsymbol{\phi}_z^{\mathrm{T}})\,\partial\Omega+\int_{\Gamma_1}\boldsymbol{\phi}(s)k_n\frac{\partial\boldsymbol{\phi}^{\mathrm{T}}(s)\,\mathrm{d}s}{\partial n}\right]\mathbf{P}_n=0 \quad (8)$$

where

$$\boldsymbol{\phi}_x=\frac{\partial\boldsymbol{\phi}}{\partial x},\quad \boldsymbol{\phi}_y=\frac{\partial\boldsymbol{\phi}}{\partial y},\quad \boldsymbol{\phi}_z=\frac{\partial\boldsymbol{\phi}}{\partial z}.$$

Given that the finite element formulation is of the order of $C^1$ with respect to the space variables, continuity of the pressure values from element to element must be met [20]. The information obtained will give values of the pressure at the various prescribed nodes. From pressure values, the velocity distribution can be obtained from a discretized Darcy's law equation (1).

*Finite element method for mass transfer*

The finite element formulation for the conservation of chemical species, equation (4), contains additional convective and time-dependent terms and is also well known [20]. In the Galerkin formulation, we let

$$C_{\mathrm{f}}(x,y,z,t)\approx C_{fn}(x,y,z,t)=\sum_{i=1}^{n}C_{fi}(t)\phi_i(x,y,z,t)=\boldsymbol{\phi}^{\mathrm{T}}\mathbf{C}_{fn}$$

$$C_{\mathrm{t}}(x,y,z,t)\approx C_{tn}(x,y,z,t)=\sum_{i=1}^{n}C_{ti}(t)\phi_i(x,y,z,t)=\boldsymbol{\phi}^{\mathrm{T}}\mathbf{C}_{tn} \quad (9)$$

and the test function

$$\delta C_{fn}=\sum_{i=1}^{n}\delta C_{fi}\phi_i(x,y,z)=\boldsymbol{\phi}_{\mathrm{T}}\delta\mathbf{C}_{fn}$$

where $\mathbf{C}_{fn}$, $\mathbf{C}_{tn}$, $\boldsymbol{\phi}$, and $\delta\mathbf{C}_{fn}$ are $n\times 1$ vectors. We obtain

$$\delta\mathbf{C}_{fn}^{\mathrm{T}}\left[\int_{\Omega}(D_x\boldsymbol{\phi}_x\boldsymbol{\phi}_x^{\mathrm{T}}+D_y\boldsymbol{\phi}_y\boldsymbol{\phi}_y^{\mathrm{T}}+D_z\boldsymbol{\phi}_z\boldsymbol{\phi}_z^{\mathrm{T}}+u\boldsymbol{\phi}^{\mathrm{T}}\boldsymbol{\phi}_x+v\boldsymbol{\phi}^{\mathrm{T}}\boldsymbol{\phi}_y+w\boldsymbol{\phi}^{\mathrm{T}}\boldsymbol{\phi}_z)\,\partial\Omega+\int_{\Gamma_1}\boldsymbol{\phi}(s)D_n\frac{\partial\boldsymbol{\phi}^{\mathrm{T}}(s)}{\partial n}\mathrm{d}s\right]\mathbf{C}_{fn}=\delta\mathbf{C}_{fn}^{\mathrm{T}}\times\left[\int_{\Omega}\boldsymbol{\phi}\boldsymbol{\phi}^{\mathrm{T}}\,\partial\Omega\right]\left[\frac{\partial}{\partial t}\left(\mathbf{C}_{fn}+\frac{V_{\mathrm{t}}}{V_{\mathrm{f}}}\mathbf{C}_{tn}\right)\right] \quad (10)$$

given the same definitions for the $\boldsymbol{\phi}_{x,y,z}$. Again the problem can be solved given the appropriate boundary conditions. The continuity conditions for this formulation are the same as for the pressure formulation and the solution is obtained in terms of the concentration of the chemical species in the fluid at the different nodes.

The formulation for the case when the mass transfer Peclet number is large is a reduction of the general equation above. The equation simplifies to

$$\delta\mathbf{C}_{fn}^{\mathrm{T}}\left[\int_{\Omega}(u\boldsymbol{\phi}^{\mathrm{T}}\boldsymbol{\phi}_x+v\boldsymbol{\phi}^{\mathrm{T}}\boldsymbol{\phi}_y+w\boldsymbol{\phi}^{\mathrm{T}}\boldsymbol{\phi}_z)\,\partial\Omega\right]\mathbf{C}_{fn}=\delta\mathbf{C}_{fn}^{\mathrm{T}}\left[\int_{\Omega}\boldsymbol{\phi}\boldsymbol{\phi}^{\mathrm{T}}\,\partial\Omega\right]\times\left[\frac{\partial}{\partial t}\left(\mathbf{C}_{fn}+\frac{V_{\mathrm{t}}}{V_{\mathrm{f}}}\mathbf{C}_{tn}\right)\right]. \quad (11)$$

Upon substitution of equation (6) for $\partial C_{\mathrm{t}}/\partial t$ in equation (11) and rearranging, the matrix equation for this finite element first-order Euler forward integration scheme becomes

$$[M]\times\mathbf{C}_{fn}^{i}+[Q]\times\mathbf{C}_{tn}^{i}=[S]\times\mathbf{C}_{fn}^{i+1} \quad (12)$$

where $[M]$, $[Q]$, and $[S]$ are $n\times n$ matrices, and the $C_{fn}$ and $C_{tn}$ are $n\times 1$ vectors. The update of the terms $C_{tn}$ depends on the numerical approximations of Fick's law. In this work, a simple first-order Euler forward integration scheme [22] is used for equation (6)

$$\mathbf{C}_{tn}^{i}=\mathbf{C}_{tn}^{i-1}+\frac{hP_{\mathrm{s}}S_{\mathrm{a}}}{V_{\mathrm{t}}}(\mathbf{C}_{fn}^{i-1}-\mathbf{C}_{tn}^{i-1}) \quad (13)$$

where $h$ is the time stepsize and $i$ the step number. Equations (12) and (13) can be solved iteratively to obtain the values for the chemical species concentration in both the fluid and tissue. A detailed derivation of the formulations given in this work can be found in ref. [22].

## SIMULATION

To illustrate the new concept in modeling, fluid flow and mass transfer is numerically analyzed in a two-dimensional representation of the liver acinus. Figure 1(a) shows Rappaport [3, 23] and Gumucio's [24] conceptualization of the liver acinus and Fig. 1(b) shows the finite element grid used for the numerical analysis. The configuration analyzed in this work is that of a terminal portal triad which runs perpendicular to the terminal hepatic venule and the area between the two blood vessels filled with sinusoids and hepatic parenchymal cells. The finite element grid attempts to simulate this geometry. Note that the grid is variable in space, but invariant in time. This particular division was used to provide comparable accuracy in both the $x$- and $y$-directions over the whole domain. The letters A, B, and C denote the radial lines along which the pressure, velocity, and chemical specie concentration are plotted. They will be referred to repeatedly in association with the simulated results.

Both the governing equations and the finite element formulations are reduced to two dimensions. In the pressure analysis, flow rate along the terminal portal vein is low. Based on typical values for velocity, vein diameter and length, the pressure drop along the vein

Table 1. Characteristic constants and parameter values

| Name | Symbol | Value | References |
|---|---|---|---|
| Pressure portal vein | $P_1$ | 6 cm $H_2O$ | 18 |
| Pressure hepatic vein | $P_0$ | 2 cm $H_2O$ | 18 |
| Porosity | $\theta_0$ | 0.11 | 17 |
| Length of sinusoid | $L_s$ | $3.0\times10^{-4}$ m | 13 |
| Diameter of sinusoid | $d_s$ | $7.0\times10^{-6}$ m | 17 |
| Surface area/volume tissue | $S_A/V_t$ | 556 $cm^{-1}$ | 16 |
| Permeability in $x$-direction | $k_{x0}$ | $4.3\times10^{-9}$ $m^4$ $N^{-1}$ $s^{-1}$ | 25 |
| Permeability in $y$-direction | $k_{y0}$ | $2.6\times10^{-9}$ $m^4$ $N^{-1}$ $s^{-1}$ | 25 |
| Characteristic velocity | $u_0$ | $3.0\times10^{-3}$ m $s^{-1}$ | 25 |
| Membrane permeability | $P_s$ | $4.8\times10^{-5}$ cm $s^{-1}$ | 1 |
| Characteristic time | $t_0$ | 50 s | |
| Specie concentration | $C_0$ | 1% vol. | |
| Kinematic viscosity | $\nu$ | $2.72\times10^{-7}$ $m^2$ $s^{-1}$ | 24 |
| Diffusion coefficient | $D_s$ | $6.7\times10^{-11}$ $m^2$ $s^{-1}$ | 1 |

is less than 5%. Since flow in the terminal hepatic vein occurs perpendicular to the plane of the figure, no pressure is expected across the vein. Thus constant pressure conditions are assumed along the terminal portal vein and in the terminal hepatic vein. The values for the pressure conditions are obtained from literature [25] and are tabulated in Table 1. Each terminal hepatic vein has fluid from several acinii which flow into it. There is intermixing of fluid along the edges of each acinus. Since each acinus encounter similar pressure boundary conditions along the terminal portal vein and in the hepatic vein, from geometric arguments the resultant net flux across this boundary is minimal. We impose an adiabatic condition along the two sides of the grid.

For the chemical species analysis, the reduced formulation of the chemical species equation (10) is used because the typical mass transfer Peclet number in the liver for some chemical species (i.e. glucose, sucrose, mannitol) is greater than 100 [15, 26]. As a result, only inlet fluid concentrations are needed to satisfy the boundary condition.

The numerical analysis is performed using dimensionless variables in order to facilitate a more general presentation of the results. Table 2 provides the definition of the dimensionless variables used in this work. The absolute variables (i.e. $x$, $y$, pressure $P$, fluid concentration $C_f$, and tissue concentration $C_t$) have been normalized with respect to characteristic constants. For example, the dimensionless pressure, $P^*$, is defined as the difference between the absolute pressure and the pressure at the hepatic vein normalized by the difference between the portal vein and the hepatic vein pressures. The other dimensionless variables are also normalized with their respective characteristic constants given in Table 1.

The following is a brief description of the numerical computation scheme. The individual grid elements were mapped into eight node isoparametric elements and a five-point Legendre–Gaussian quadrature scheme was used for the numerical integration [20]. A halving method for grid reduction was used to determine the appropriate grid spacing. The finite element scheme provides an accuracy of the order of $\delta x^2$ and $\delta y^2$ locally and $\delta x$ and $\delta y$ globally [20].

The equations were solved on a VAX 11/750 minicomputer. The complete computer program can be found in ref. [22]. The following procedure was employed in the simulation. First, the pressure and velocity values at the nodes were determined from the solution of equation (9). Then the velocities of the fluid were incorporated into the reduced conservation

Table 2. Dimensionless numbers and variables

| Name | Symbol | Expression |
|---|---|---|
| Reynolds | $Re_{d_s}$ | $u_0 d_s/\nu$ |
| Peclet | $Pe_m$ | $u_0 d_s/D_s$ |
| Pressure | $P^*$ | $P(x,y)-P_0/P_1-P_0$ |
| Velocity | $V^*$ | $V(x,y)/u_0$ |
| Time | $t^*$ | $t/t_0$ |
| Concentration | $C^*_{f,t}$ | $C_{f,t}(x,y,t)/C_0$ |
| $x$-Direction | $X^*$ | $x/L_s$ |
| $y$-Direction | $Y^*$ | $y/L_s$ |
| Permeability in $x$-direction | $k_x$ | $k_x(x,y)/k_{x0}$ |
| Permeability in $y$-direction | $k_y$ | $k_y(x,y)/k_{y0}$ |

† f is the fluid and t the tissue.

of species equation (12) to determine the chemical species concentration in the fluid and tissue. Given that influx fluid concentration is known for each time step, the concentration distribution could be determined provided the time-dependent term is known. The time-dependent term is evaluated simultaneously with the solution to equation (12) from the Euler integration of Fick's law. Since this numerical scheme is explicit, the solution marches forward in time from one time step to another. As a result, an automatic time step controller is used to prevent instability from occurring. The chemical species distribution was then calculated simultaneously for each element in both the fluid and the tissue.

## RESULTS AND DISCUSSION

Solutions are obtained from the numerical scheme for the fluid flow and chemical species distribution in the two-dimensional geometric representation of the liver acinus. This study includes a parametric investigation of the effects of hydraulic permeability on the pressure and velocity distribution. The hydraulic permeability has physical significance and its effect on pressure and velocity distribution are important. It is known that flow through the sinusoids traverse a tortuous path [23]. If the tortuosity and porosity of the acinus remain the same throughout the acinus, then the permeability remains a constant. However, studies have shown that towards the hepatic vein, the path becomes more radially converging and the cross-sectional area of the sinusoids increases [6, 27]. Both these changes would increase the hydraulic permeability.

This study also investigates the dynamic response to a step change in the chemical species concentration flowing into the liver acinus. The step response will provide information on the two-dimensional chemical species distribution in the tissue and the fluid as well as the concentration variation in the effluent. Overall these results should provide insight into the sensitivity of the model to the various parameters as well as a better physical understanding of the multi-dimensional mass transfer process in the liver acinus.

### *Effects of hydraulic permeability on pressure and fluid velocity*

Figure 2 is obtained from the solution of equation (9). It shows a plot of constant pressure (isobaric) lines throughout the acinus with three varying hydraulic permeabilities: a constant permeability 1.0, a linearly increasing permeability from 1.0 to 1.2, and a linearly increasing permeability from 1.0 to 1.5. There is a pressure drop of 0.1 dimensionless pressure between each set of lines from the inlet (terminal portal venule) to the outlet (terminal hepatic venule). This figure shows the two-dimensional behavior of the pressure distribution, which from the imposed boundary conditions is symmetric about the centerline. Note that for a given hydraulic permeability, the relative distances between isobaric lines decrease from the inlet to the outlet. This would indicate that the pressure gradient becomes steeper close to the outlet. For a given pressure, the constant hydraulic permeability isobaric line is located closer to the inlet than lines with a linearly increasing permeability. Although the variation in permeability does not shift the isobaric lines significantly, the pattern of the shift is regular. This behavior of the pressure distribution is more easily seen in Fig. 3.

Figure 3 is a plot of the pressure along the three radial lines A, B, and C as a function of the dimensionless distance $x^*$. They represent the center, the periphery, and an area midway between the two. The results are for two different hydraulic permeabilities: the constant permeability and the linearly increasing permeability from 1.0 to 1.2. Note that the pressure drop along the centerline, C, is almost linear. However, along the periphery, A, the initial slope of the pressure line is almost zero, and it ends with a very steep drop toward the outlet. The nonlinearity of the pressure lines is a function of position within the acinus. This accounts for the two-dimensional distribution of the pressure. The shapes of these curves resemble qualitatively those obtained from experimental measurements [25].

The effects of a varying permeability can also be seen in this figure. At a given axial location, the linearly increasing hydraulic permeability pressure is less than the constant permeability pressure. Along C, the pressure gradient becomes more linear. Along A, the initial slope is steeper, and the outlet pressure drop is not as large. Again, the shifts in pressure lines are not significant, but the pattern is regular.

Figure 4 shows the fluid velocity distribution and the effects of the variable hydraulic permeability on the distribution. The curves represent the magnitude of the flow velocities along the same radial lines as the pressure curves in Fig. 3. Again, note that the velocities are not uniform and display a wide range of values. The magnitude of the velocity is the product of the first derivative of the pressure along the path length and the hydraulic permeability (Darcy's law). Note that the velocities close to the inlet are lower in value than the velocities near the outlet. This would qualitatively be consistent with the predictions from previous experimental studies [6, 27]. The plot shows that the velocity along the centerline, C, is almost a constant near the inlet and gradually increases toward the outlet. At the periphery, the fluid velocity along A initially is almost zero, which coincides with almost no pressure drop near the inlet. Since the curvature of the pressure plot is greater for the periphery than along the other radial lines, the velocity increases sharply toward the outlet.

The effects of the hydraulic permeability on the velocity of the fluid can also be seen in this figure. This is best illustrated by the velocity along radial line C. The flow with an increasing hydraulic permeability

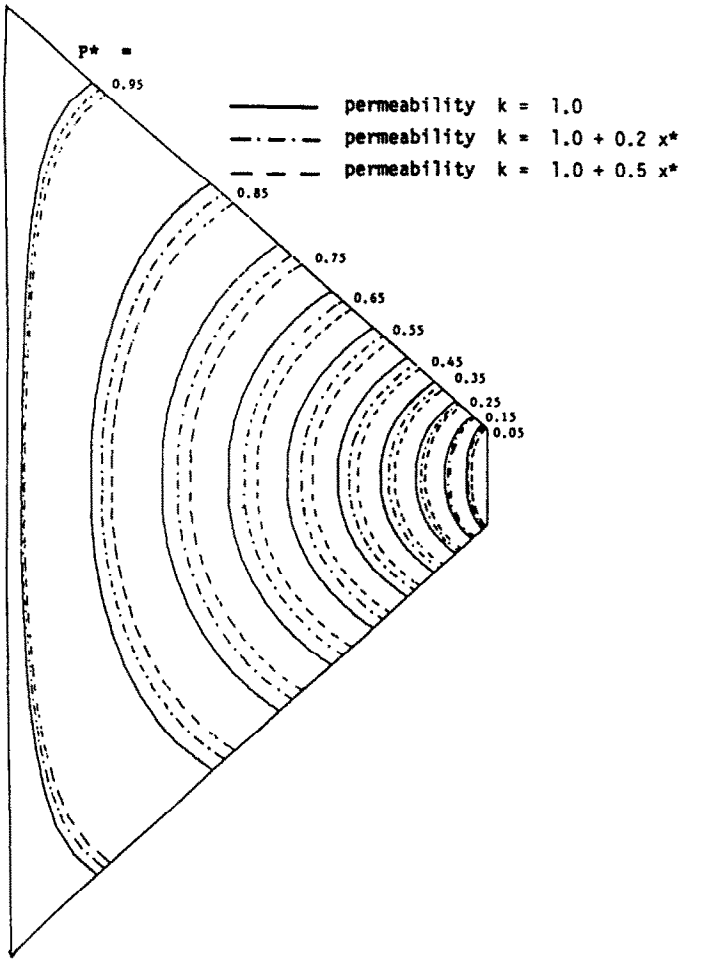


FIG. 2. Plot of isobaric lines in liver acinus with increments of $0.1P^*$. The different line styles represent a constant permeability of 1.0, a linearly increasing permeability from 1.0 to 1.2, and a linearly increasing permeability of 1.0 to 1.5.

starts at a higher velocity than the flow with a constant permeability. This corresponds to a larger pressure gradient near the inlet. Toward the outlet, even though the pressure gradient is less for the increasing permeability, the velocity is still higher. This occurs because the permeability is linearly increasing. These results illustrate the importance of the microvascular structure in controlling the fluid flow in the liver acinus. This part of the study also demonstrates the potential of this new model to study and understand in greater detail the flow properties in the hepatic acinus.

*Response to step change in inlet chemical species concentration*

The remainder of this study deals with mass transport in the liver. We will present results for the fluid and tissue concentration distribution in the liver acinus for a step change in the inlet species concentration from 0 to 1. Figure 5 shows the isoconcentration lines in the fluid 0.10 dimensionless time after the step change in the inlet condition. Each line represents an equal increment of species concentration from the inlet to the outlet. Note that the concentration of chemical species in the fluid is nonuniform and exhibits a two-dimensional behavior. For a particular concentration, the location for that concentration close to the centerline occurs further downstream than for those areas close to the periphery. Near the periphery, the species concentration in the fluid is nearly depleted a short distance away from the inlet.

The effect of such a distribution on the tissue can be readily seen in Fig. 6 which is a plot of isoconcentration lines in the tissue also 0.10 dimensionless time after the step change. Close to the inlet, the areas away from the centerline have an overall higher tissue concentration. A transition does occur toward the middle of the acinus where the centerline concentration exceeds that of the surrounding fluid. This behavior is a direct result of the distribution of the chemical species in the fluid. From Fig. 5, the concentration gradient in the fluid close to the inlet is

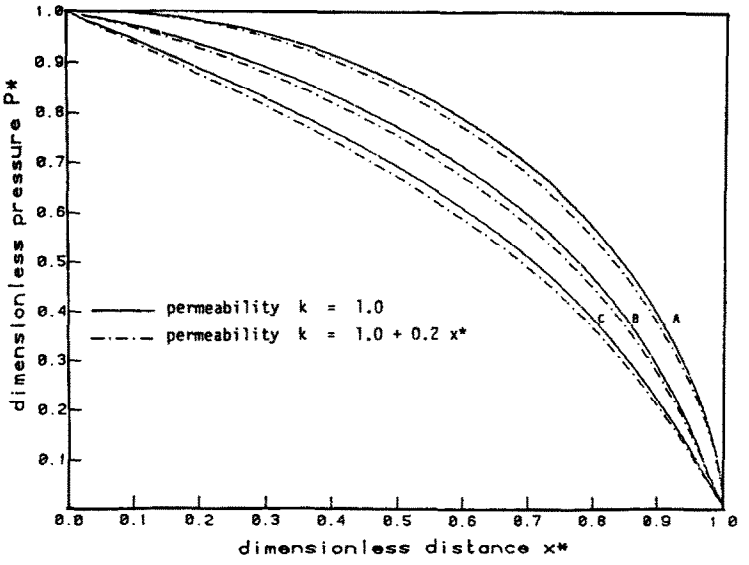


FIG. 3. Plot of dimensionless pressure $P^*$ vs dimensionless $x^*$ along radial lines A, B, and C. The different line styles represent a constant permeability of 1.0 and a linearly increasing permeability from 1.0 to 1.2.

quite sharp for areas near the periphery. This would indicate that the concentration in the fluid has depleted rapidly and is transported into the tissue across the cell membrane. Therefore, the tissue concentration in that region will be relatively high. The centerline concentration gradient in the fluid is more gradual, as a result, a lower tissue concentration occurs in areas near the inlet. However, the depletion of the chemical species in the fluid near the periphery results in a low tissue concentration further downstream. Areas close to the centerline do not have this problem because the chemical species do not deplete so drastically.

At later times, the behavior of the concentration distribution changes. Figure 7 shows the isoconcentration lines in the fluid after 1.0 dimensionless time has elapsed. The shapes of the lines are quite different from those at 0.1 dimensionless time. Now, the centerline concentration is lower than for areas in the surrounding fluid. The shapes of the curves are all

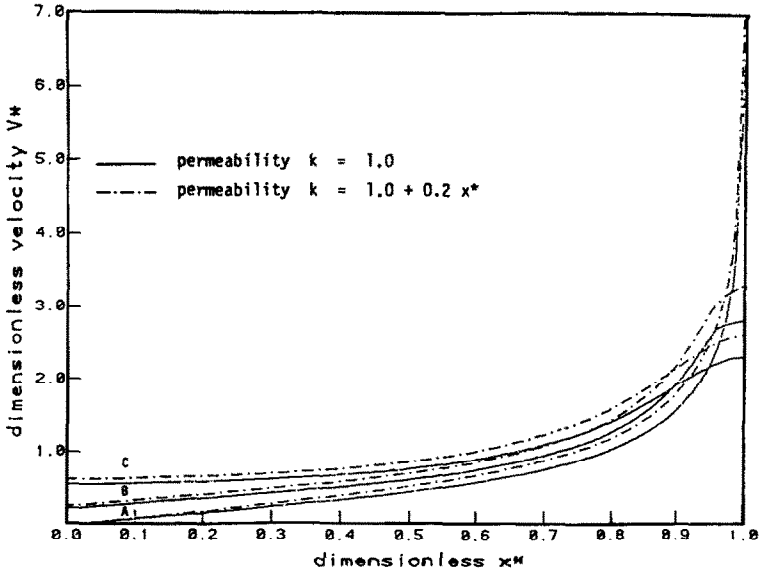


FIG. 4. Plot of dimensionless velocity $v^*$ vs dimensionless $x^*$ along radial lines A, B, and C. The different line styles represent a constant permeability of 1.0 and a linearly increasing permeability from 1.0 to 1.2.

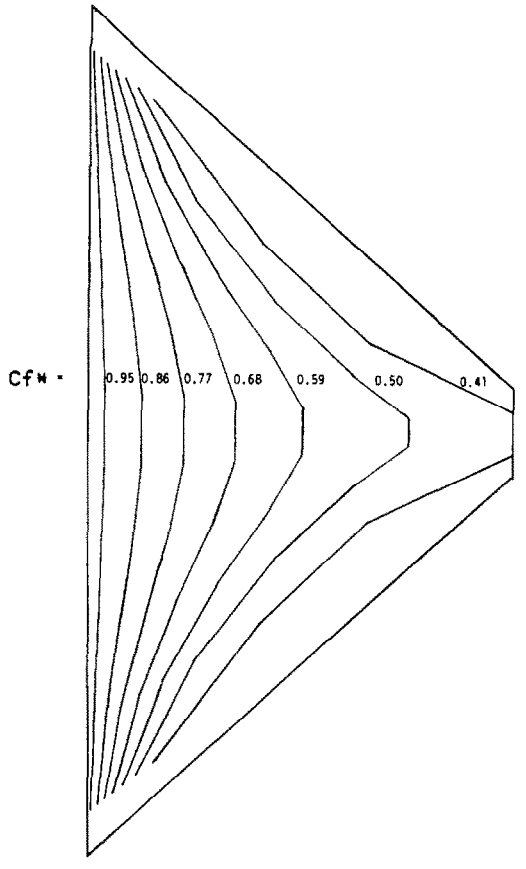


FIG. 5. Plot of isoconcentration lines in the fluid for step change in inlet concentration at 0.1 dimensionless time.

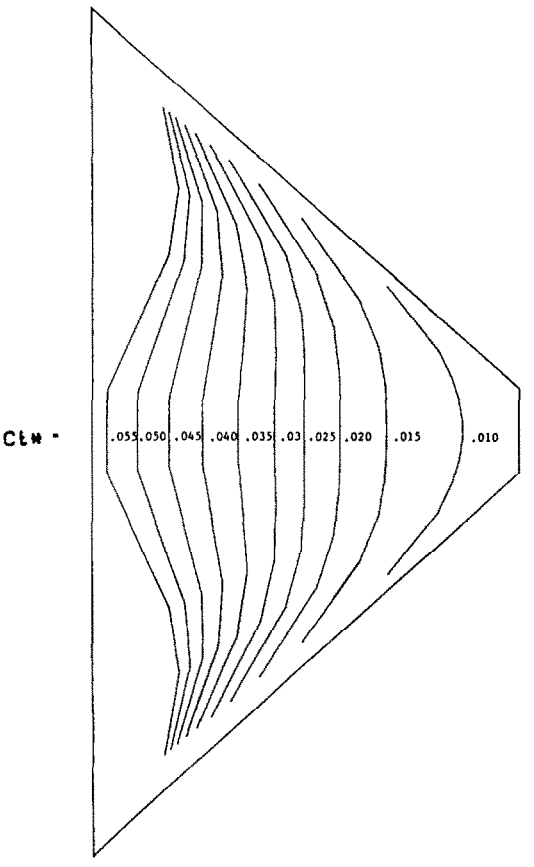


FIG. 6. Plot of isoconcentration lines in the tissue for step change in inlet concentration at 0.1 dimensionless time.

rather regular with the periphery experiencing the highest fluid concentration. The curvatures of the lines remain circular even close to the outlet.

Figure 8 shows the tissue isoconcentration lines for the same time. The shapes of the curves resemble those in the fluid. A high fluid concentration usually results in higher mass transfer to the tissue. Thus, the centerline concentration is lower than the surrounding areas. Again, the periphery experiences the highest concentration. Note however that toward the outlet, the curvature of the tissue isoconcentration begins to flatten whereas previously it was observed that the fluid isoconcentration line remained circular.

The previous four figures show that the concentration distribution of the species in both the fluid and tissue remains nonuniform and two-dimensional following a step increase in concentration in the fluid perfusing the liver acinus. Figure 9 is a plot of the fluid concentration during the step response vs the dimensionless distance $x^*$ from the inlet along two radial lines, A and C, and at three different times 0.1, 1.0, and 2.0. The curves representing the concentration along radial line A initially have a rapid decay. Then later in time, the fluid concentration in areas close to the inlet have reached the inlet condition and the shape of the curve becomes more sigmoidal. Along radial line C, the concentration appears almost linear. Note that at early times, the centerline concentration is substantially higher than the peripheral concentration, and at later times, the peripheral concentration exceeds the centerline. This is consistent with the plots of the fluid isoconcentration in Figs. 5 and 7. A transition occurs between the times 0.1 and 1.0 where the peripheral concentration near the inlet is higher than the centerline, but the opposite is true near the outlet.

In Fig. 10, the tissue concentration is plotted vs the dimensionless distance $x^*$. The same location and times used are the same as those used in Fig. 10. At a dimensionless time of 0.10, the concentration along the periphery near the inlet is higher than the concentration in the corresponding area along radial line C. There is, however, a crossover point in which the centerline concentration is higher than at the periphery. At later times, this crossover point travels toward the outlet. The periphery and centerline concentration near the outlet at these times are approximately equal, which is consistent with the isoconcentration curve near the outlet in Fig. 8. Note also, that there is a significant drop in tissue concentration near the outlet. The drop is much more prominent for the periphery than for the centerline.

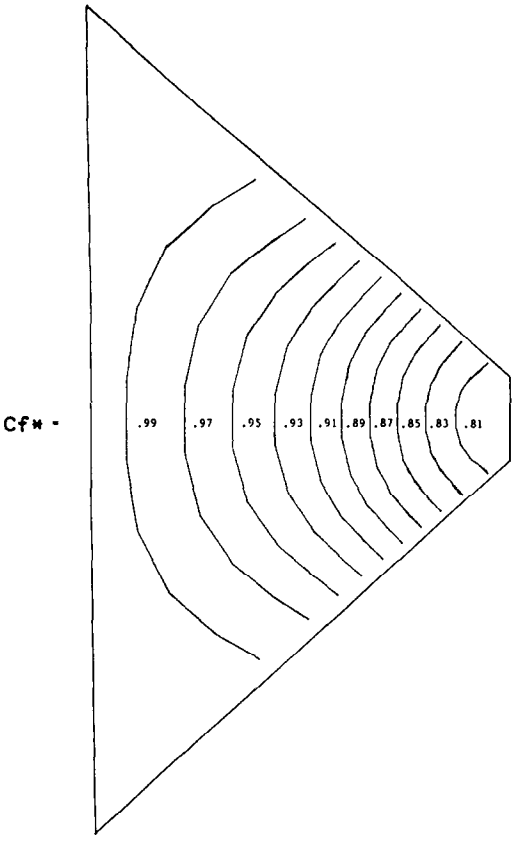


FIG. 7. Plot of isoconcentration lines in the fluid for step change in inlet concentration at 1.0 dimensionless time.

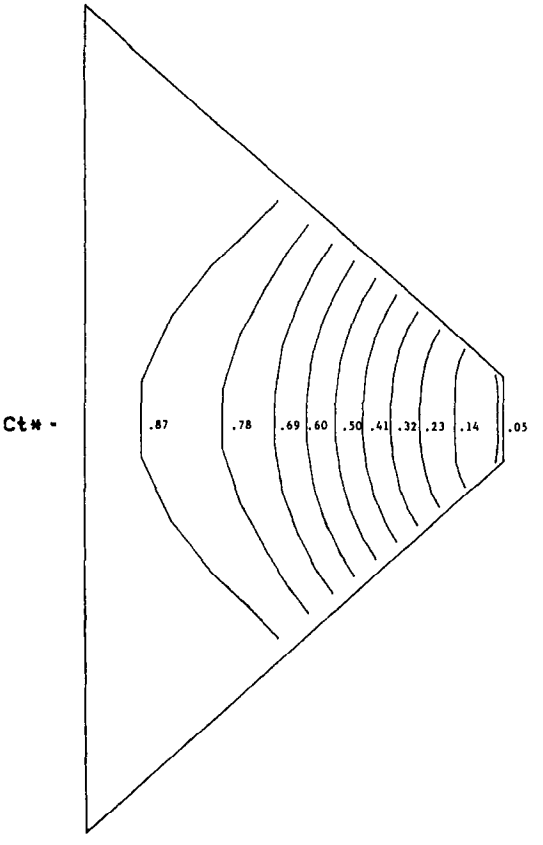


FIG. 8. Plot of isoconcentration lines in the tissue for step change in inlet concentration at 1.0 dimensionless time.

*Factors which influence the concentration distribution*

The particular variations of the fluid and tissue concentration following a step change in inlet conditions are a result of three factors: the local flow rate, the path length, and the mass transfer rate into the tissue. The effects of these factors at earlier times were seen in Figs. 5 and 6. The flow rate at the inlet decreases from the centerline to the periphery. The path length increases from the centerline to the periphery for an equal increment in the $x$-direction. As a result, the fluid flow transit times increase from the centerline to the periphery. At early times, this is coupled with a uniform mass transfer rate near the inlet resulting in more mass transfer to the tissue in areas away from the centerline. This effect will decrease the fluid concentration rapidly in the area close to the periphery. Further downstream, the low fluid concentration at the periphery results in a decreased mass transfer rate. At later times, the areas of slower flow rate become enriched with the chemical species and this allows the tissue downstream to experience higher fluid concentration. Thus, the mass transfer rate is increased significantly downstream. Figures 3–10 demonstrate that the mass transport process from the fluid perfusing the liver acinus into the cells is a time-dependent phenomena. The results show clearly that the species concentration in the tissue is multi-dimensional with a distribution that changes as a function of time. Even so, the mass transfer to the tissue does not increase significantly near the outlet because the tissue concentration in that area does not show a significant difference between the periphery and the centerline. This would account for the near uniform concentration observed in this region in Fig. 9. The process of chemical species accumulation by the tissue, however, takes time and the concentration in the effluent does not always reflect this delay.

Figure 11 is a plot of the effluent concentration vs time following a step input. This curve is very similar to those observed from both experimental data (unpublished results) and results simulated from other models [9]. Note that the effluent concentration is really a composite of the different fluid concentrations at the outlet of the acinus. Thus the complexity of the multi-dimensional transient mass transfer process in the liver, observed in Figs. 3–10 is not always reflected by the effluent concentration.

## CONCLUSION

The goal of this paper was to introduce a new concept in modeling fluid flow and mass transfer in the liver utilizing principles from porous media theory.

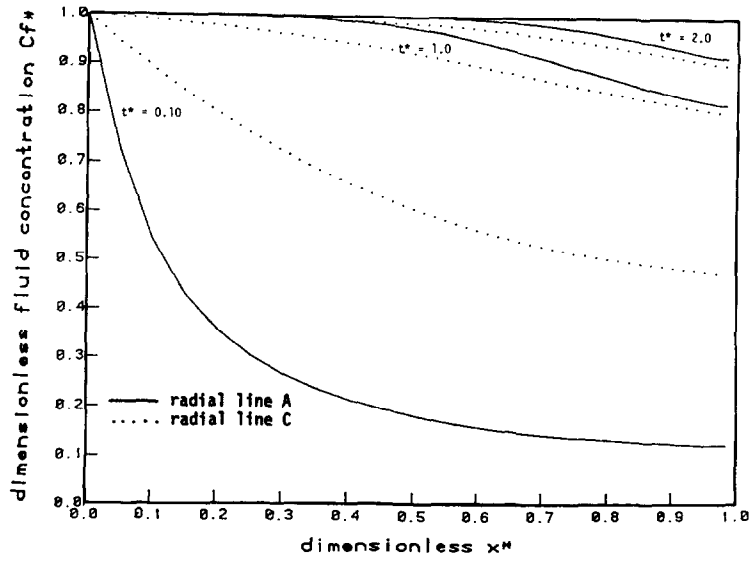


FIG. 9. Plot of dimensionless fluid concentration vs dimensionless $x^*$ along radial lines A and C at 0.1, 1.0, and 2.0 dimensionless time. The different line styles represent values along radial line A and radial line C.

We illustrated this new concept by applying it to a two-dimensional representation of the liver acinus. The results indicated that fluid flow through the acinus is not one-dimensional and not at a constant velocity as proposed by other models. Rather fluid flow in the acinus is a complex multi-dimensional flow with a wide variation in velocities. This affects the mass transfer process in the liver acinus resulting in a multi-dimensional transient chemical species distribution in both the tissue and the perfusing fluid. The results from this study provide a better understanding of the effects of hydraulic permeability on fluid flow and the mass transfer process.

This work is an initial step in the modeling of fluid flow and mass transfer in the liver acinus. Even though a two-dimensional model has illustrated the complexity of the acinus, a three-dimensional model will eventually be needed in order to provide a more complete understanding of fluid and mass transfer at this level. A complete understanding of the distri-

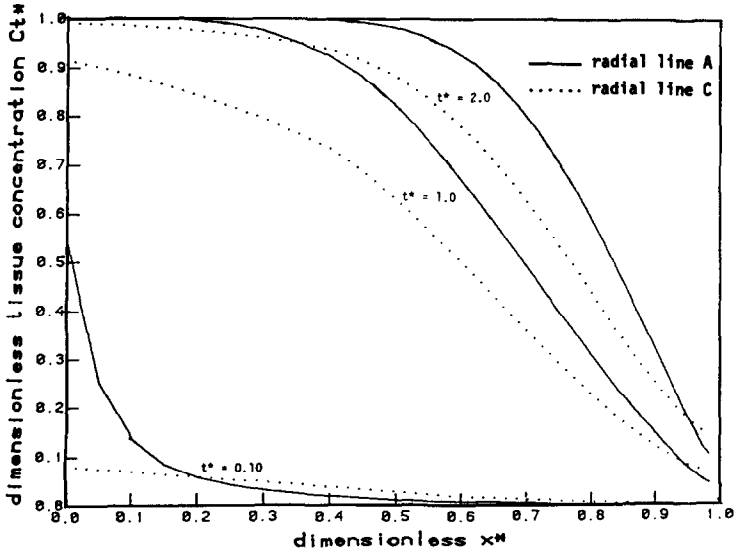


FIG. 10. Plot of dimensionless tissue concentration vs dimensionless $x^*$ along radial lines A and C at 0.1, 1.0, and 2.0 dimensionless time. The different line styles represent values along radial line A and radial line C.

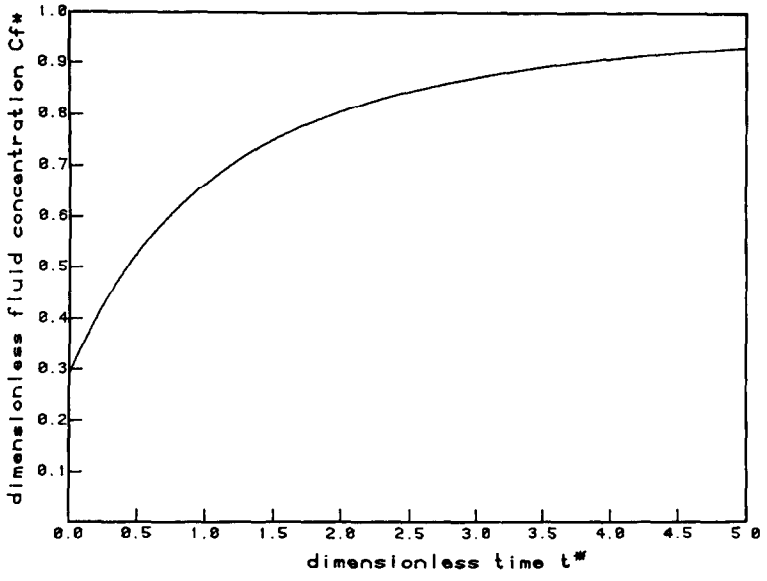


FIG. 11. Plot of the effluent concentration vs dimensionless time.

bution of the liver acinii throughout the liver is also needed.

This paper presented a simple diffusion mass transfer process across the cell membrane governed by Fick's law. There are many other modes which can be incorporated into the model with relative ease. For example, these modes can include mass transfer rates determined by metabolism or irreversible thermodynamics.

Further work in this area will require analysis of a three-dimensional geometry of the hepatic acinus, a distribution of the acinii within the liver, and a more general mass transfer law. Once this is accomplished, this model can be a powerful tool in determining chemical species distribution throughout the liver and in understanding further the hepatic uptake process.

## REFERENCES


1. I. M. Arias, H. Popper, D. Schachter and D. A. Shafritz (Editors), *The Liver: Biology and Pathobiology*, pp. xxiii–xxv. Raven Press, New York (1983).
2. C. I. Smith and T. C. Merigan, Therapeutic approaches to chronic hepatitis B. In *Progress in Liver Diseases* (Edited by H. Popper and F. Schaffner), Vol. VII, pp. 481–494. Grune & Stratton, San Francisco, California (1982).
3. A. M. Rappaport, The microcirculatory hepatic unit, *Microvascular Res.* **6**, 212–228 (1973).
4. J. Gumucio, D. L. Miller, M. D. Kraus and C. C. Zanolli, Transport of fluorescent compounds into hepatocytes and resultant zonal labeling of the hepatic acinus in the rat, *Gastroenterology* **80**, 639–646 (1981).
5. J. J. Gumucio and D. L. Miller, Zonal hepatic function: solute hepatocyte interactions within the liver acinus. In *Progress in Liver Diseases* (Edited by H. Popper and S. Fenton), Vol. VII, pp. 17–30. Grune & Stratton, San Francisco, California (1981).
6. A. Koo, Y. S. Liang and K. K. Cheng, The terminal microcirculation in the rat, *J. Exp. Physiol.* **60**, 261–266 (1975).
7. K. S. Pang and M. Rowland, Hepatic clearance of drug: I. Theoretical considerations of a "well-stirred" model and a "parallel tube" model. Influence of hepatic blood flow, plasma, and blood cell binding, and the hepatocellular enzymatic activity on hepatic drug clearance, *Pharm. Biopharm.* **5**, 625–640 (1977).
8. K. Winkler, S. Keiding and N. Tygstrup, Clearance as quantitative measure of liver function. In *The Liver: Quantitative Aspects of Structure and Function* (Edited by G. Paumgartner, R. Preisig and S. Karger), pp. 144–155. Basel (1973).
9. C. A. Goresky, G. G. Bach and B. E. Nadeau, On the uptake of materials by the intact liver: the concentrative transport of rubidium-86, *J. Clin. Invest.* **52**, 975–990 (1973).
10. L. Bass, R. Robinson and A. J. Bracken, Hepatic elimination of flowing substrates. The distributed model, *J. Theor. Biol.* **72**, 161–184 (1978).
11. M. S. Roberts and M. Rowland, Hepatic elimination–dispersion model, *J. Pharm. Sci.* **74**, 585–587 (1985).
12. P. Motta, M. Muto and T. Fujita, *The Liver: an Atlas of Scanning Electron Microscopy*. Igaku-Shorin, Ltd., Tokyo (1978).
13. A. E. Scheidigger, *Physics of Flow through Porous Media*. University of Toronto Press, Toronto (1974).
14. W. M. Rohsenow and H. Choi, *Heat, Mass, and Momentum Transfer*, pp. 10–12. Prentice-Hall, Englewood Cliffs, New Jersey (1961).
15. W. M. Kays and M. Crawford, *Convective Heat and Mass Transfer*, p. 277. McGraw-Hill, New York (1981).
16. J. Crank (Editor), *The Mathematics of Diffusion*, p. 10. Clarendon Press, Oxford (1979).
17. C. A. Goresky and B. E. Nadeau, Uptake of materials by the intact liver: the exchange of glucose across the liver cell membrane, *J. Clin. Invest.* **53**, 634–646 (1974).
18. A. L. Lehininger, *Biochemistry: The Molecular Basis of Cell Structure and Function*, p. 125. Worth, New York (1978).
19. O. Kedem and A. Katchalsky, Thermodynamic analysis of the permeability of biological membranes to non-electrolytes, *Biochim. Biophys. Acta* **27**, 22–244 (1958).
20. J. N. Reddy, *An Introduction to the Finite Element Method*. McGraw-Hill, San Francisco, California (1985).
21. S. D. Conte and C. de Boor, *Elementary Numerical*

*Analysis: an Algorithm Approach*, pp. 354–362. McGraw-Hill, San Francisco (1980).
22. C. Y. C. Lee, Multi-dimensional analysis of heat and mass transfer in the liver, Ph.D. dissertation (1989).
23. A. M. Rappaport, Hepatic blood flow. In *Liver and Biliary Tract Physiology I* (Edited by N. B. Javilt), pp. 1–63. University Park Press, Baltimore, Maryland (1980).
24. J. J. Gumucio, Functional and anatomic heterogeneity in the liver acinus: impact on transport, *Am. J. Physiol.* **244** (Gastrointest. Liver Physiol., 7), G578–G582 (1983).
25. K. Nakata, C. F. Leong and R. W. Brauer, Direct measurement of blood pressures in minute vessels of the liver, *Am. J. Physiol.* **199,** 1181–1188 (1960).
26. G. Alpini, R. A. Garrick, M. J. T. Jones, R. Nunes and N. Tavolini, Water and nonelectrolyte permeability of isolated rat hepatocytes, *Am. J. Physiol.* **251**(Cell Physiol. 20), C872–C882 (1986).
27. D. L. Miller, C. S. Zanolli and J. J. Gumucio, Quantitative morphology of the hepatic acinus, *Gastroenterology* **76,** 965–969 (1979).

## UN MODELE MULTIDIMENSIONNEL DE QUANTITE DE MOUVEMENT ET DE TRANSFERT DE MASSE DANS LE FOIE

**Résumé**—On introduit un nouveau concept dans la modélisation multidimensionnelle de l'écoulement fluide et du transfert de masse dans le foie en utilisant la théorie des milieux poreux. A partir de ce modèle, on obtient une distribution de pression et de vitesse pour le fluide en microvasculation. Les vitesses du fluide sont alors introduites dans une équation multidimensionnelle de la concentration des espèces chimiques. Une distribution de la concentration des espèces chimiques dans le fluide et le tissu est alors déterminée en utilisant une équation qui décrit le mécanisme de transfert de masse à travers la membrane de la cellule. Pour déterminer la sensibilité du modèle, on conduit quelques études paramétriques qui incluent les effets de l'architecture vasculaire sur la distribution de pression et de vitesse, et la réponse à un changement en échelon de la concentration des espèces chimiques à l'entrée.

## EIN MEHRDIMENSIONALES MODELL DES IMPULS- UND STOFFTRANSPORTS IN DER LEBER

**Zusammenfassung**—Diese Arbeit stellt ein neues Konzept zur Darstellung mehrdimensionaler Strömungen und des Stofftransports in der Leber vor. Kenntnisse über das Verhalten poröser Medien werden verwendet, um die Druck- und Geschwindigkeitsverteilung in der Mikrogefäßstruktur zu berechnen. Die Fluidgeschwindigkeiten werden in die mehrdimensionalen Erhaltungsgleichungen für die Stoffkonzentration eingesetzt. Mit einer weiteren Gleichung, die den Stofftransport durch die Zellmembran beschreibt, wird die Verteilung der Stoffkonzentrationen in der Flüssigkeit und im Gewebe bestimmt. Verschiedene Parameter-Studien werden durchgeführt, um die Sensibilität des vorgestellten Modells zu bestimmen. Dabei werden die Einlüsse der Gefäß-Architektur auf Druck- und Strömungsverteilung sowie die Reaktionen auf schrittweise Änderungen der Stoffkonzentrationen berücksichtigt.

## МНОГОМЕРНАЯ МОДЕЛЬ ПЕРЕНОСА ИМПУЛЬСА И МАССЫ В ПЕЧЕНИ

**Аннотация**—Представлена новая концепция моделирования многомерного течния жидкости и массопереноса в печени, основанная на положениях теории пористых сред. С помощью предложенной модели получены распределения давления и скорости жидкости в микрососудистой системе. Найденные значения скорости жидкости подставляются затем в многомерное уравнение сохранения химических веществ. Далее с использованием уравнения, описывающего процесс массопереноса через клеточную мембрану, рассчитывается распределение концентрации химических веществ в жидкости. Для установления адекватности модели проведен ряд исследований, включающих анализ влияния структуры сосудов, а также ступенчатого изменения начальной концентрации химических веществ на распределение давления и течение в печени.